Journal of Alloys and Compounds 728 (2017) 126–137

Contents lists available at ScienceDirect

Journal of Alloys and Compounds

journal homepage: http://www.elsevier.com/locate/jalcom

Scratch adhesion strength of plasma sprayed carbon nanotube reinforced ceramic coatings

Sudhakar C. Jambagi

Department of Mechanical Engineering, National Institute of Technology Karnataka Surathkal, Mangaluru, Karnataka state, 575025, India

ARTICLE INFO

Article history:
Received 3 July 2017
Received in revised form
25 August 2017
Accepted 28 August 2017
Available online 31 August 2017

Keywords:
A. Ceramics
A. coating materials
B. chemical synthesis
C. Microstructure
D. Mechanical property
D. Scanning electron microscopy (SEM)

ABSTRACT

This report investigates the effect of both mechanical and thermal properties of Carbon nanotube (CNT) on scratch adhesion strength of ceramic coatings. Micro sized alumina and titania with 1 wt% CNT powders were prepared by three routes: dry/wet milling (with alcohol) and heterocoagulation. First, degree of CNT dispersion in the coatings was analysed. Heterocoagulated coatings displayed homogeneous dispersion of CNT. Next, the effect of homogeneous dispersion on phase transformation was studied. Higher thermal conductivity of CNT and its degree of dispersion seemed to affect the melting of powders and thus the phase transformations in the coatings. A higher fraction of stable phase was detected in the coatings. In addition, CNT/ceramic interface was analysed for the reaction layer. A stable phase layer was found covering the entire CNT surface, protecting it from thermal degradation. Finally, the scratch adhesion strength was quantified for both CNT reinforced and unreinforced coatings. The scratch resistance of heterocoagulated coatings improved by ~36–176%. Improvement in strength was attributed to: a) a higher stable phase fraction in the coatings, b) Strong wettability at CNT/ceramic interface, c) improvement in elastic moduli of the coatings has also led to the improvement in the work of adhesion of the coatings, and d) a toughening mechanism, CNT bridging.

1. Introduction

Plasma spraying is a thermal spray process wherein the powder feedstock is simultaneously heated and accelerated towards substrate by plasma jet. The molten or semi-molten particles impinged on the substrate to form a layer. Deposition of such multiple layers yields a coating of the desired thickness [1,2].

Plasma sprayed titania and alumina coatings are well known for their sliding wear resistance owing to their superior mechanical properties [3]. Titania coatings were less hard (~850 ± 50 HV) than alumina coatings (~1200 $HV_{0.3}$) [4,5]. In addition, the phases present in the coating govern their properties for e.g., in the case of titania coating, the rutile phase was a stable phase that exhibits better mechanical properties, similarly, α-alumina has been a desirable phase in alumina coatings [6,7]. Titania coatings are employed on the light bearing, pump seals and engine cylinders under moderate load conditions [8,9]. On the other hand, alumina coatings were employed under heavy duty conditions to protect printing rollers in paper making industry and in hydraulic pump plungers and valves [1].

Multiwalled carbon nanotube (MWCNT) has been a promising reinforcement for ceramic coatings due to their superior mechanical properties; however, a strong agglomeration tendency of the reinforcement poses the challenge of uniform dispersion in the powders and coatings. Unless otherwise specified, in this report, MWCNT referred as CNT. Agarwal and his team have reported extensively on plasma sprayed Al_2O_3/CNT coatings [10,11]. From their reports, following conclusions can be drawn: 1) CNT was protected in the plasma plume. 2) With just 1.5 wt% CNT, ~15% improvement in hardness, and with 4 wt% CNT, ~43% improvement in fracture toughness were achieved through the toughening mechanisms like CNT bridging and CNT pull-outs [10]. Nevertheless, the majority of the reports dealt with Ar-He plasma gas, the powders were prepared by spray drying technique, and the CNT content was varied in 1.5 to 8 wt% the range. Recently, He et al. [9] reported on the mechanical properties of plasma sprayed titania/3 wt%CNT coatings. The powder precursor was prepared by spray drying process. Subsequently, the plasma sprayed coatings have shown improvement in their hardness, elastic modulus, and fracture toughness around 38.5%, 34.2% and 54.9%, respectively. This was attributed to toughening mechanisms like CNT bridging and

E-mail address: sudhakar@nitk.ac.in.

http://dx.doi.org/10.1016/j.jallcom.2017.08.262
0925-8388/

crack deflection. In addition, the CNT was protected by the titania layer, but this report failed to provide detailed insight on TiO_2/CNT interface, which defines the interfacial bond strength and hence responsible to improve the coating properties. Heterocoagulation, a colloidal processing technique, however, is gaining importance these days for its good dispersion capability of CNT, especially in micron-sized ceramic powders [12,13].

The phase transformation in plasma sprayed coatings has been analyzed by Rietveld refinement analysis. Several operating parameters seems to affect the phase transformation. Gualtieri et al. [14] considered the effect of only a set of parameters. On the other hand, Sabiruddin et al. [5] quantified the stable phase in plasma sprayed alumina considering the effect of standoff distance, primary and secondary gas flow rate, nozzle size. However, the transformation from α to γ or to other phases was deliberately suppressed in order to obtain good mechanical properties of the coatings [5].

A Few reports available on the study of phase transformation of titania coatings. Wang et al. [15] investigated the effect of Ar–He–H2 and Ar–He–N2 plasma gases on anatase phase fraction. The anatase phase fraction was in 10 –22.5 wt% range. The phase fraction was found to decrease with an increase in primary gas flow rate, and it has resulted in poor mechanical properties.

Owing to high thermal conductivity of CNT (~3000 W/mK), it was envisaged that the CNT might affect the degree of melting of coatings and hence it might affect the phase transformation in the coatings. There are no reports yet highlighting these aspects of CNT reinforced ceramic coatings, especially considering the effect of CNT dispersion.

The scratch test has been a simple method to assess adhesion strength of plasma sprayed ceramic coatings. Hazra and Bandyopadhyay [16] investigated the scratch resistance of conventional and nano-structured alumina coatings using a Rockwell C indenter. The coating failure in these cases was attributed to tensile cracking, leading to a large area spallation. Nanostructured coatings had higher scratch resistance as compared to the conventional coatings, and this was attributed to its bimodal microstructure. No previous study has investigated the adhesion strength of TiO_2/CNT coatings.

In the current work, it should be pointed out that a N_2-H_2 gas mixture is used as plasma gas, which is significant as far as the economics of spraying is concerned, and the CNT concentration was limited to 1 wt%. Micro sized crushed titania and agglomerated alumina powders were used in this investigation. The CNT doped powders were prepared using three methods: dry mixing, wet mixing and heterocoagulation. These powders were used to deposit coatings. The study focusses on the following four aspects of the coatings. First, the dispersion status of CNT in the coatings is investigated. Second, the CNT and its dispersion influence on phase transformation was studied. Third, the CNT/ceramic interface was examined for a possible reaction layer. Finally, the scratch adhesion strength of the coatings was examined considering the effects of CNT dispersion, phases present in the coatings, and the CNT/ceramic interface.

2. Experimental procedure

2.1. CNT doped powder preparation

The powders used in this investigation along with their particulars are listed in Table 1. In this study, CNT with an average diameter in the range 10–20 nm and length 1–2 μm (JK Impex, Mumbai, India) was used. The purity of this CNT, as reported by the manufacturer, is 97%. The 1 wt% CNT doped powders were prepared using three different techniques, namely, dry mixing, wet mixing, and a heterocoagulation. Dry mixing refers to ball milling of CNT/ceramic powder without any crushing media. On the other hand, wet mixing refers to the ball milling in presence of ethanol. The detailed procedure of powder preparation was discussed in Jambagi et al. [12]. The powders and coatings are designated based on the type of processing technique followed and CNT concentration in them. For e.g. the titania powder processed by dry mixing (DM) method with 1 wt% CNT was designated as DMT1. Similarly, when the crushed titania powder was processed through wet mixing (WM), it was designated WMT1, and when the same powder was synthesized by heterocoagulation(H), it was designated as HT1. Similarly, DMA1, WMA1, and HA1 represent dry mixed, wet mixed and heterocoagulated agglomerated alumina powders/coatings (with 1 wt% CNT), respectively. The powders morphology was studied using scanning electron microscope (SEM) (EVO 60, Zeiss, Jena, Germany). The as received crushed titania (Metco 102) and agglomerated alumina powders and their corresponding coatings were referred as HT0 and HA0, respectively.

2.2. Coating deposition and characterization

The coatings were deposited on C 20 plain carbon steel substrate using a 40 kW plasmatron (Metco 3MB, Westbury, NY, USA) mounted on a CNC XY table. The coatings were fabricated using the parameters listed in Table 2. On grit blasted sample, around 100 μm thick Ni-5Al bond coat followed by 400 μm top coat was deposited. For microstructural study, the coatings were sliced to a size 10 mm × 10 mm × 5 mm using low diamond saw. These slices were mounted in Bakelite mould followed by polishing using SiC papers and diamond pastes with decreasing diamond grit size. The polished cross sections were examined under a scanning electron microscope (SEM) (EVO 60, Zeiss, Jena, Germany).

2.3. CNT dispersion in the coating

Raman imaging was carried out using Raman spectrometer (LabRAM HR800, JobinYvon Horiba, Villeneuve-d'Ascq, France), also operated at excitation wavelength of 532 nm. A CNT peak at 1100 cm^{-1} reported by Rao et al. [17] was selected for Raman imaging purpose. The detailed procedure of Raman imaging technique has been explained in our earlier report [13].

2.4. Properties of coatings

Elastic moduli of the CNT reinforced coatings were measured using depth sensing indentations. The indentations were performed using an instrumented hardness tester (Micro combi tester (MCT), CSM instruments, Switzerland) equipped with Vickers indenter. These measurements were undertaken under a maximum load of 3000 mN, loading and unloading rate of 6000 mN/min and with a dwell time of 15 s. Moduli of elasticity of the coating were then obtained from the slope of unloading curve [18]. An average of ten readings was reported.

2.5. Rietveld analysis of the coatings

X-ray diffraction (XRD) analysis was carried out to identify the phases present in the coating followed by Rietveld analysis. This was done using X-ray diffractometer (PW 1729 generator and PW 1710 goniometer, Phillips, Amsterdam, Netherlands) generating Cu Kα radiation. X ray data collected on as-sprayed coatings operated at 30 kV and 40 mA. JCPDS data files were used to identify the peaks. Quantitative phase analysis of the coatings was done using Rietveld analysis. The analysis was carried out using PANalytical High score Plus software. During Rietveld refinement, structure models of each phase corresponding to XRD data were retrieved

Table 1
Powders used in the investigation.

Name	Size (μm)	Composition (wt%)	Type	Manufacturer and description
Top coats				
Agglomerated alumina	−90 + 45 Individual platelet size: 0.5–5	Al_2O_3 > 99.4	Agglomerated	M/S Hindalco, India (HT)
Crushed Titania	−45 + 11	TiO_2 > 99	Fused and crushed	M/S Sulzer Metco, USA, (102)
Bond coat				
Nickel Aluminium	−90 + 45	Ni 95, Al 5	clad	M/S Sulzer Metco, USA, (450 NS)

Table 2
Representative Plasma spray parameters.

	Standoff distance (mm)	Voltage (V)	Current (A)	Primary gas (slpm)	Secondary gas (slpm)	Power (kW)
Alumina	125	64	500	N_2(50)	H_2(5)	32
Titania	125	60	500	N_2(50)	H_2(5)	30

from ICSD data library. Refinement was performed to get a goodness of fit (GOF) by adjusting the parameters like scale factor, flat background, zero shift, lattice parameters, half width, orientation parameters, atomic coordinates (x, y, z), U V W, peak shape parameters etc.

2.6. CNT/titania interfacial study

The CNT/titania coating interface was studied under a high-resolution transmission electron microscope (HRTEM) (JEM 2100, JEOL, Tokyo, Japan). For this purpose, the coating was removed from the substrate using a low-speed diamond saw and a 3 mm diameter sample was taken out for further processing. This sample was polished using fine grade polishing papers to a thickness of around 100 μm. Next, the sample was placed on a dimple grinder (Gatan 656, Pleasanton, CA, USA) where a crater of 1 mm diameter was created in the middle of the sample and the thickness of the sample in the ground area was further reduced to around 50 μm. In the following step, the sample was polished using a precision ion polishing system (Gatan 691, Pleasanton, CA, USA) so as to reduce the sample thickness to 20 μm in the pre-ground area (dimple).

2.7. Scratch test

Top thickness of the coating was first ground to 50 μm and then polished to a roughness of ~1 μm Ra using the procedure explained in the report [13]. Scratch test was performed using a scratch tester (TR-101-M5, Ducom, Bangalore, India) equipped with a Rockwell C type conical indenter having an apex angle of 120° and a tip radius of 200 μm. Consequently, the scratch test was performed above under a variable load in 30–100 N range. Scratching speed and distance were 0.1 mm/s and 7 mm, respectively. Three scratches were made on each sample. The critical load and work of adhesion were calculated for each of these scratches and the average value is reported along with standard deviation. The locations of coating failure and failure mechanism were examined using a SEM (JSM, Jeol, Tokyo, Japan). A Field emission scanning electron microscopy (FESEM) was used to capture the images of CNT elements embedded on the scratch track.

3. Results and discussion

3.1. Powder morphology and the XRD analysis of powders

Fig. 1(a) shows the secondary electron image of crushed titania powder (Metco 102). This powder was produced by crushing and grinding and therefore it has an angular and blocky appearance. The XRD peaks for this powder is shown in Fig. 1(b). The as-received powder contained magneli and rutile phases (Fig. 1(b)). Fig. 1(c) shows the secondary electron image of the as-received agglomerated alumina and is composed of platelets of size in the 0.5–1 μm range. This powder is constituted by the α phase, i.e., a stable hcp phase of common occurrence. The stable phase peaks are shown in the XRD plot of this powder (Fig. 1(d)). From Fig. 1(a) and (c), it can be observed that the agglomerated powders are larger than titania powders. It may be noted that the agglomerated alumina powder is composed of a number of smaller platelets, with size ranging from 0.5 to 2 μm (Fig. 1(c)). This means that these platelets have a size slightly larger than the nanostructured powders. Hence, the microstructure of this coating has a similarity with that produced from a nanostructured powder. Being porous, these platelets restrict heat transfer during coating, thereby creating partially melted regions in the coating. Hence, it is obvious that the smaller particles undergo complete melting than the larger particles [19]. This aspect especially holds good for agglomerated alumina powders that enables the coatings to retain α phase, which has lower interfacial energy [5].

3.2. Coating microstructure

Fig. 2 shows SEM images of microstructures of HT0 and HA0 coatings. Both coatings exhibited good microstructural integrity and are free from cracks at the interface. Moreover, the porosity values of HT0 and HA0 coatings were reported as 3.8 ± 0.9 and 9.1 ± 0.4%, respectively [13]. Thus, the HT0 coating was relatively denser than HA0 coating. Aside from powder particle size, crushed titania powder possess lower melting point (~1843 °C) than agglomerated alumina powder (~2072 °C) and hence they are expected to undergo complete melting [20]. In fact, Lima and Marple [4] reported 2.5 ± 0.4% porosity of plasma sprayed crushed titania coatings whereas agglomerated alumina porosity has been reported to lie in the range 5–9.4% [21]. Furthermore, the HA0 coating typically behaves like a nanostructured material and exhibit bimodality i.e., partially melted (PM) and fully melted (FM) regions in its microstructure as shown in the inset of Fig. 2(b). Microstructure of such a nature was expected of such powders and has been dealt in the report by Sabiruddin et al. [22].

3.3. CNT retention and dispersion in the coating

The viscosity of molten pure titania is unknown. However, Bessinger [23] has claimed the viscosity of slags containing 80 wt% titania around 30 mPa s at the temperature above 1600 °C while the melting point of pure titania is 1843 °C. Hence, possibly the viscoity

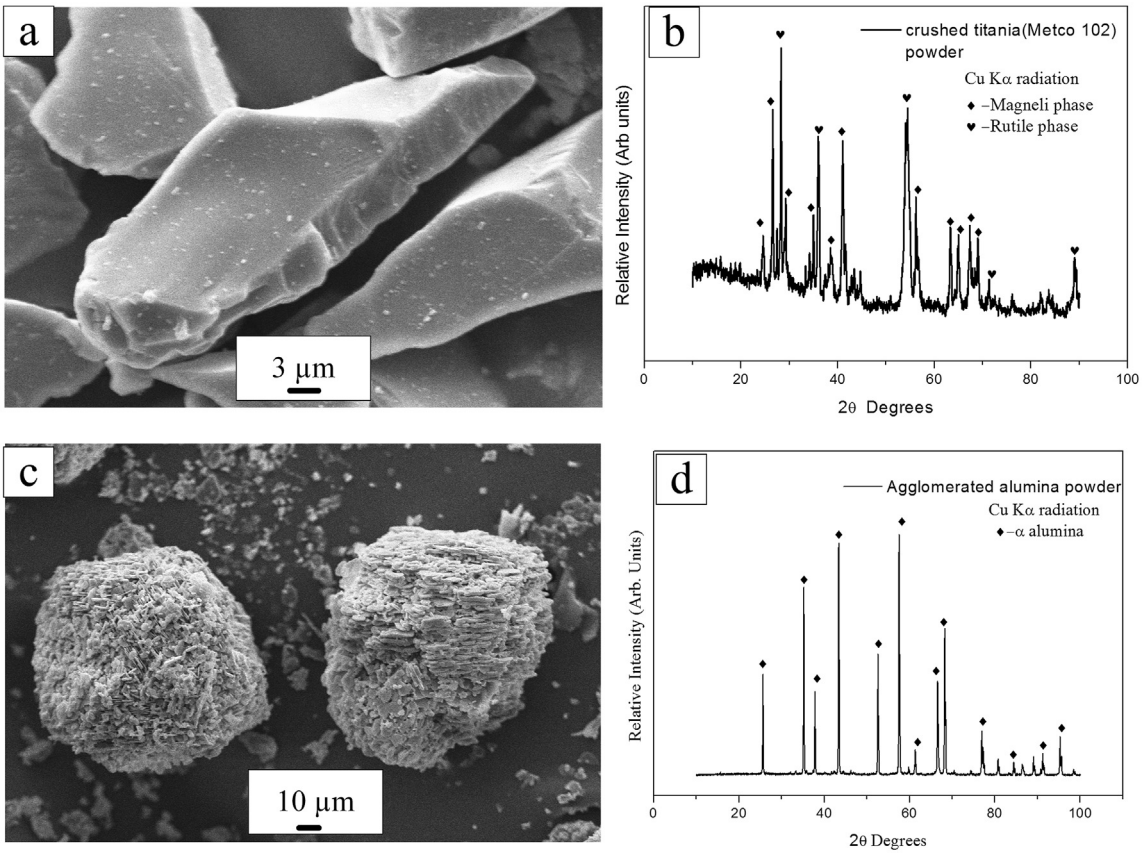

Fig. 1. Secondary electro image showing powder morphology of (a) HT0 and (c) HA0 and their corresponding XRD plots are shown in (b) and (d), respectively.

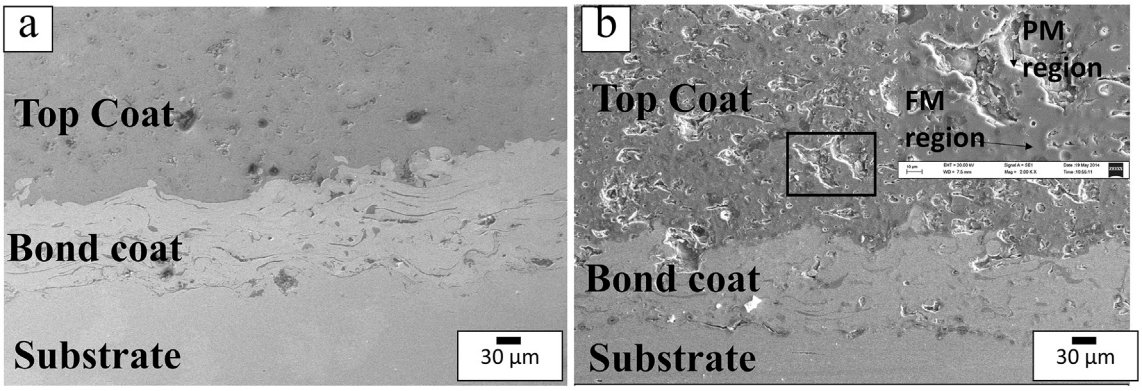

Fig. 2. Secondary electron image showing polished cross section of (a) HT0 and(b) HA0 coatings.

of molten titania is much lower than that of alumina. Such a low viscosity of titania might have promoted its spreading on the CNT elements by capillary action and enabled to get properly wet CNT. Such infiltration of titania and its dense coating can further challenge the CNT characterization using Raman spectroscopy. However, the CNTs were characterised using HRTEM and is explained in section 3.6.

Crushed alumina (Metco 105 NS) is another powder that resembles crushed titania (Metco 102) in its morphology because this powder was also prepared by crushing and grinding. Since relatively dense coating was resulted for titania, it has been, therefore, made difficult to capture the CNT characteristic peaks, namely, D and G peaks, in Raman spectroscopy. Hence, the CNT retention for the case of crushed alumina coating may be conveniently recalled here [13]. Previous report [13] has revealed the conspicuous G peak in the heterocoagulated crushed alumina coatings that indicated the possible retention of CNT in these type of coatings.

The dispersion of CNT in the titania coatings has been analysed using Raman imaging technique. Fig. 3 shows the Raman images for DMT1 and HT1 coatings. The bluish dots correspond to CNT and red background correspond to the matrix phase. In DMT1 coating, the CNTs tend to form agglomerates and form CNT-rich regions (Fig. 3(a)). Such effects were reported by Balani et al. [10] for CNT-doped alumina powders prepared by ball milling process (Fig. 3(a)). On the other hand, heterocoagulation was successful in extricating the individual CNTs through functionalization process. As a result, a homogeneous dispersion of CNT in the matrix for heterocoagulated coating (HT1) is obtained as illustrated in Fig. 3(b). A CNT

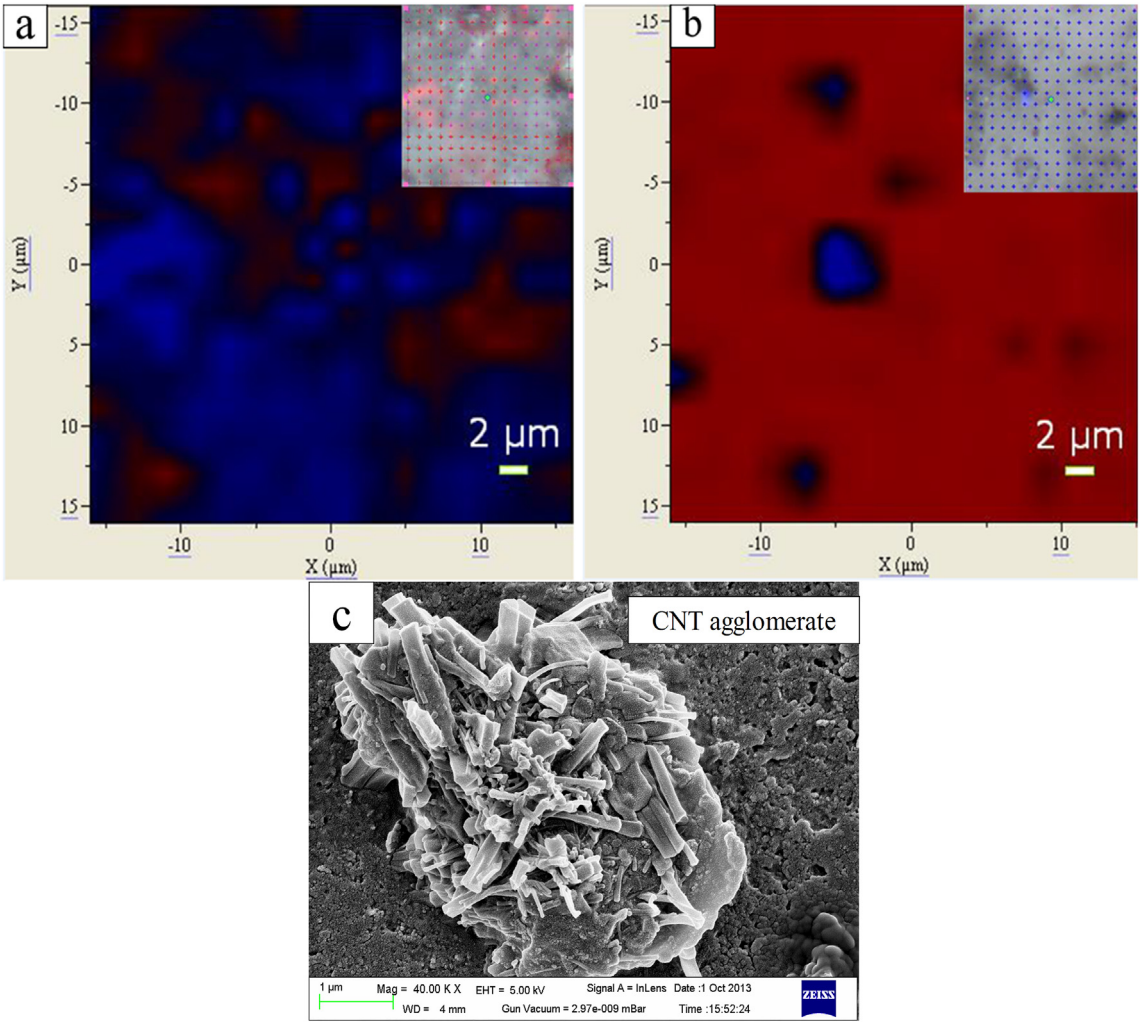

Fig. 3. Raman imaging showing the degree of dispersion of CNT in (a) DMT1, (b) HT1 coatings and (c) An SEM image of a CNT agglomerate in DMA1 coating.

agglomerate was identified in dry mixed agglomerated alumina coating (Fig. 3(c)). Such CNT agglomerates exists in wet mixed coatings as well, their size, however, was relatively smaller due to the debundling effect of ethanol [12].

3.4. Primary coating properties

Elastic moduli and Poisson's ratio of CNT reinforced coatings were estimated using Halpin Tsai model and the calculation procedure is explained in the following section. This model proposed the following relations for the estimation of the elastic modulus of composite with fibre reinforcement. Additionally, this model provides a good approximation for short and randomly oriented fibres [24,25].

$$\frac{M}{M_m} = \frac{1 + \varsigma\eta V_f}{1 - \eta V_f} \quad (1)$$

$$\eta = \frac{\left(\frac{M_f}{M_m}\right) - 1}{\left(\frac{M_f}{M_m}\right) + \varsigma} \quad (2)$$

where,

M = composite material modulus of elasticity/Poisson's ratio

Mf, Mm = corresponding fibre and matrix modulus/Poisson's ratio, respectively.

ξ = Shape factor, i.e., a measure of fibre reinforcement of the composite, that depends on fibre geometry, packing geometry, and loading conditions. For CNT, it is the L/D ratio of the CNT elements (ξ = 100 see section 2.1.)

In this model, elastic moduli values of alumina, titania and CNT were assumed as 300 [26], 230 [27] and 1000 GPa [28], respectively; Poisson's ratio of these powders was assumed as 0.22 [29], 0.25 [30] and 0.55 [31], respectively.

3.5. Phase transformation in the coatings

Since the phase fractions in as received titania powder (Metco 102) was unknown, first, this powder was subjected to Rietveld analysis. Result shows that as received powder contained only 24.9% rutile and rest magneli phase (Fig. 4(a)). Subsequently, the powders were plasma sprayed using the powder manufacturer recommended parameters (Table 2). As stated earlier, the crushed titania coatings were dense and their XRD analysis (not shown) showed only rutile phase. The transformation to rutile phase has been an instantaneous process. In fact, with initial plasma power of ~30 KW, the coatings depicted only a rutile phase. Earlier reports,

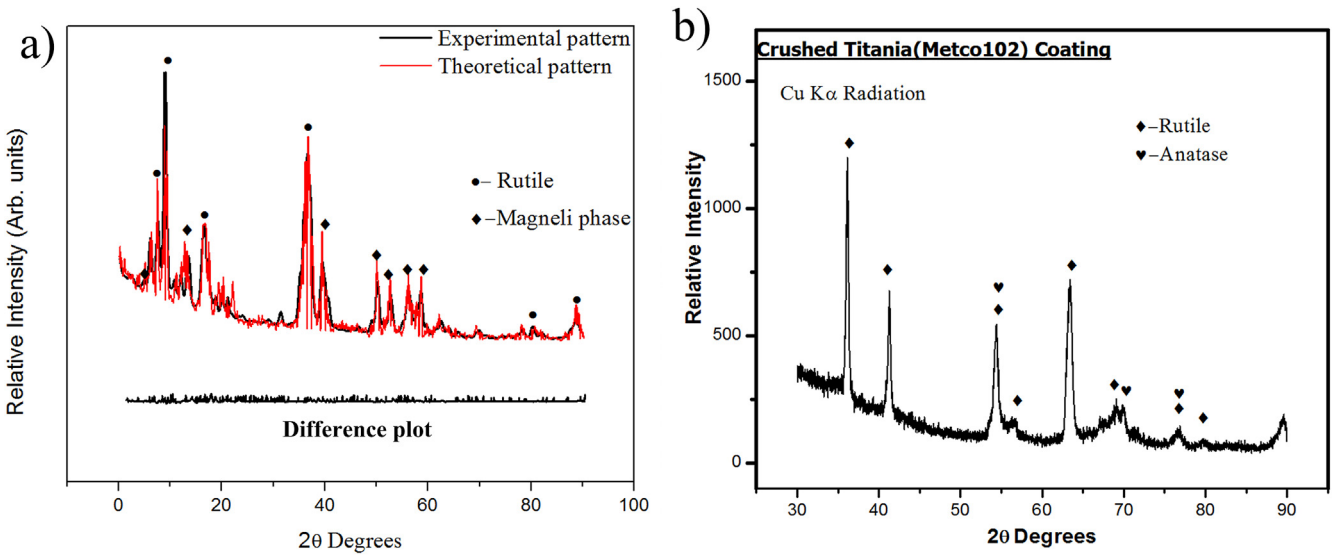

Fig. 4. Experimental and theoretical pattern plot of (a) crushed titania powder and (b) XRD plot of corresponding coating.

revealed an interesting fact that the transition temperature for stable rutile phase had lied in ~600–700 °C range in air under the absence of any dopants [32]. This implies that the transformation would be more obvious and instantaneous for high-temperature processes like plasma spray. In addition, reducing atmosphere and other impurities can also accelerate the possibility of transformation to rutile phase [33]. In order to perform Rietveld analysis, at least two phases must coexist in the coating. Hence, in the next iteration, the arc power was reduced to 26 KW. As a result, HT0 showed a few anatase peaks along with rutile phase peaks, Fig. 4(b). Lee et al. [34] have suggested a lower heat inputs to obtain anatase phase. The coatings were deposited using low plasma power to study the role of CNT as a dopant in the crushed titania powder that possibly influences the phase transformations in the coatings [4].

Fig. 5 summarizes the Rietveld refinement results for crushed titania coatings deposited at 26 KW power and agglomerated alumina coatings were deposited at 32 KW power. The results can be explained with the help of four points marked in Fig. 5. In Fig. 5(a), Point 1 corresponds to HT0 coating and it shows the 100% rutile transformation owing to peculiar nature of powder precursor as explained earlier. Point 2 corresponds to DMT1 coating where a lower fraction of stable phase resulted, indicating a possibility of lower degree of melting. Owing to the inhomogeneous distribution of CNT (Fig. 3(c)), CNT rich regions in the coating soak excess amount of heat than that of CNT depleted regions. This leads to a nonuniform melting of the coating. Furthermore, for thermally sprayed ceramic coatings, the agglomerated state of CNT in the coating draws more amount of heat and accelerates the solidification process, causing formation of more fraction of metastable phases in the coatings [35]. As a result, rutile phase fraction in the coating reduces. This could be attributed to a clear case of inhomogeneous distribution of CNT in the coatings. On the other hand, WMT1 coating as remembered in its powder stage has shown possible debundling of CNT and had a slightly better dispersion than DMT1 coating [13]. This is confirmed by point '3' in Fig. 5(a) where phase has been transformed to rutile. Point 4 (corresponding to HT1 coating) depicts once again 100% rutile formation. This could be an evidence of homogeneous dispersion of CNT in the coating, leading to a uniform heating of the coating and therefore the metastable phases are transformed into a stable rutile phase.

Agglomerated alumina coatings have also shown similar trend in their phase fractions (Fig. 5(b)). As stated earlier, such coatings exhibit bimodality (Fig. 2(b)). This is because the powders were typically larger in size and demand more heat to melt completely, but incomplete melt gives rise to the nucleation of stable phase i.e., α-alumina phase. However, CNT clusters (shown in Fig. 3(c)) present in DMA1 coatings (point 2) soak an excess amount of heat to melt and transform the initial phase from α to γ. This could also be an evidence of accelerated solidification, and is attributable to the role played by the bundled CNT in extracting heat from the coating. Such a process of rapid solidification and its implications on phase transformations has been explained by Aruna et al. [35]. Also, points 3 and 4 of Fig. 5(b) follow similar trend to that of Fig. 5(a) for titania coatings. However, it is important restate the fact that the WMA1 coatings also showed the CNT clustering though the cluster size (not shown) has been slightly smaller than that of DMA1 coatings due to the debundling effect of ethanol [12]. Amongst the three types of coatings, heterocoagulated coatings have outperformed on two counts: 1) homogenous dispersion of CNT was obtained in the coatings; and 2) the stable phases, namely, rutile and α alumina phases were retained in HT1 and HA1 coatings, respectively. These phases are known for their good mechanical properties [4,5] and the coatings with these stable phases are, therefore, expected to perform better under wear prone conditions.

Balani and Agarwal [11] reported on the surface temperature of the powder particles prepared by ball milling or spray drying. The higher thermal conductivity of CNT seemed to influence high heat carrying capacity of the powder particles. Owing to the presence of agglomerated CNT, ball milled powder seemed to absorb higher amount of heat which might lead to a higher degree of melting. On the other hand, spray dried powder offered a homogeneous dispersion of CNT in the ceramic powder, and thereby it experiences a lower thermal exposure inhibiting the superheating of CNT. In particular, ball milled powders exposed to a higher temperature and that possibly led to a severe degradation of CNT as reported by Jambagi et al. [13]. However, owing to homogeneous dispersion of CNT in spray dried powders, uniform heating of coating might expose the CNT to a lower temperature, which may possibly help to preserve the CNT in good condition. This hypothesis can be further corroborated by Raman imaging results obtained for the crushed titania system (Fig. 2) in which the homgeneous dispersion of CNT is depicted. Finally, it can be concluded that the coatings obtained

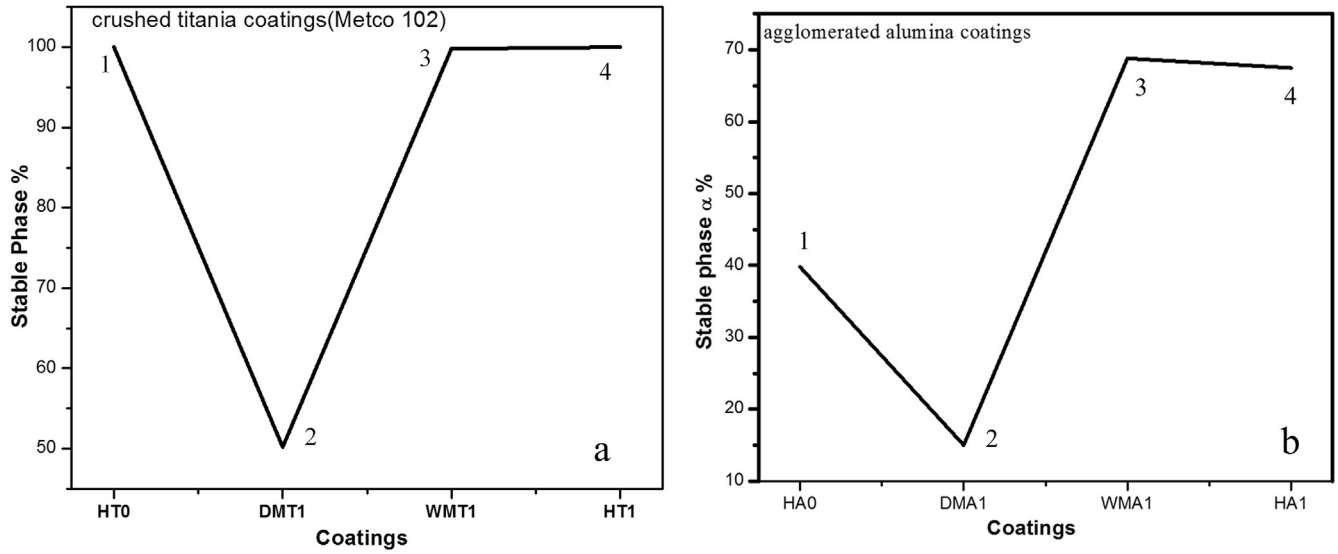

Fig. 5. The graph showing variation of fraction of stable phase with the coatings formed using various powder processing techniques for (a) crushed titania (Metco 102) coatings and (b) agglomerated alumina coatings.

using ball milled powders may result in either in higher or lower degree of the melt and consequently, a lower the amount of stable phase is formed in the coatings.

Table 3 lists the major refined parameters for various coated samples and Metco 102 crushed titania powder. It indicates how best the calculated pattern matches with the experimental pattern during refinement. From the above discussion on phase transformation, the following conclusions can be drawn: (1) the CNT, in addition to its reinforcement, it can even act as a heat sink, and (2) with a higher degree of dispersion of CNT, more stable phase fraction could be retained in the coatings. Further, these phases in large fraction would benefit the mechanical properties of the coatings.

3.6. Study of CNT/titania interface

Fig. 6 shows HRTEM image of HT1 coating highlighting important features present at the CNT/titania interface. Fig. 6(a) shows the formation of Y-junction of CNTs in the matrix. Fig. 6(b) shows an interface layer of 1.71 nm thickness, which depicts the wetting of CNT wetted by molten titania [9,36]. The top titania layer shrouds the CNT and protects against harsh plasma plume. Fig. 6(c) shows the selected-area electron diffraction (SAED) pattern corresponding to the interfacial layer marked in Fig. 6(b). SAED pattern confirms the crystalline structure of the layer. d_{hkl} corresponding to r1 and r3 as marked in the figure are calculated using the following equation: $rd_{hkl} = L\lambda = 40.183$ mm nm, where 40.183 is a given camera constant. The calculated values of d spacing corresponding to r1 and r3 are 0.20435 nm and 0.16835 nm, respectively. The hkl values corresponding to these rings are (210) and (211) and correspond to the rutile phase (ICDD ref code: 01-078-1510, ICSD: 62679). Formation of a similar stable layer has been reported for CNT/Al_2O_3 composite prepared by Keshri et al. [37]. Fig. 6(d) also shows the presence of an amorphous zone adjacent to the CNT. This area has been marked using a circle and the corresponding SAED pattern has been shown in the inset in the same figure. Hanaor and Sorrel [32] investigated phase transformation of titania from anatase to rutile in presence of carbon. It has been observed that the following phases are likely to emerge in presence of carbon; oxygen deficient compound (TiO_{2-x}), suboxide like TiO or titanium Carbide (TiC). Kim and Kang [38]

Table 3
The major refined parameters for different coated sample.

Coating	ICDD code	ICSD code	R (expected)/%	R (profile)/%	R(weighted profile)/%	R (bragg)/%	GOF	d static
Crushed titania (Metco 102) coatings								
Metco 102 powder	01-089-8300	35123	17.00740	13.69575	17.67803	9.29	1.08	0.0489
	00-050-0790	88623				8.37		
HT0	01-075-1748	31321	–	–	–	–	–	–
DMT1	01-089-0552 01-072-1471	82081	6.38395	6.54692	8.62934	9.89	1.82	0.0653
		17009	6.38395	6.54692	8.62934	1.47	1.82	
WMT1	01-071-0650	009161	6.23276	5.781	9.10793	12.78	2.13	0.0477
	01-084-1285	202242	6.23276	5.781	9.10793	1.36	2.13	0.0477
HT1	01-089-0554	082085	–	–	–	–	–	–
Agglomerated alumina coatings								
HA0	01-082-1399	75479	6.15026	6.81650	9.10247	2.76	2.19	0.497
	01-077-0396	39014	6.15026	6.81650	9.10247	2.58	2.19	0.497
DMA1	00-010-0173	60419	6.48960	7.85268	10.25402	2.96	2.49	0.485
	01-079-1557	66558	6.48960	7.85268	10.25402	2.65	2.49	0.485
WMA1	01-080-0786	68591	6.26267	6.18063	8.29581	4.44	1.75	0.0561
	01-077-0403	39104	6.26267	6.18063	8.29581	5.55	1.75	1.754
HA1	01-078-2426	63647	6.24069	7.15553	9.46229	3.93	2.29	0.434
	01-077-0396	39014	6.24069	7.15553	9.46229	3.66	2.29	0.434

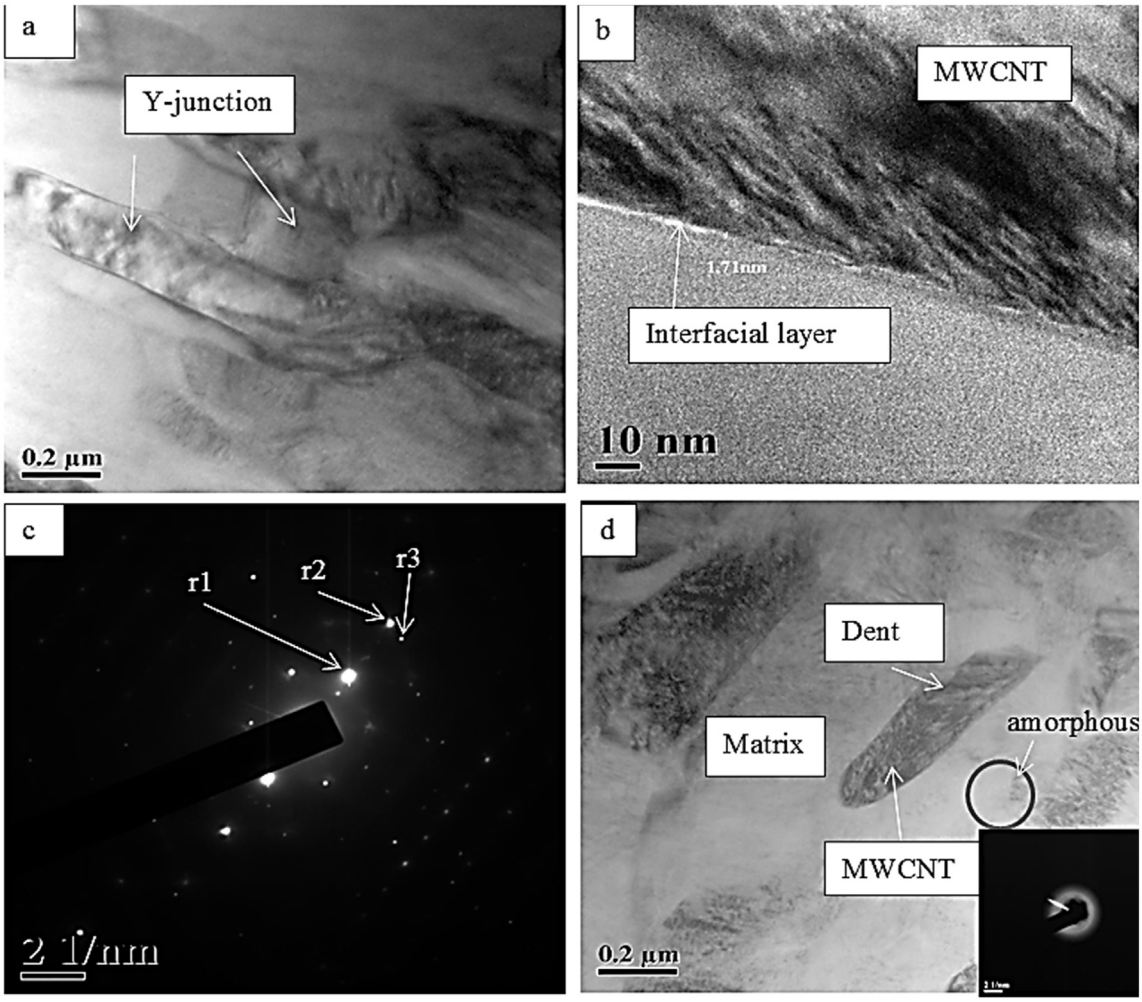

Fig. 6. HRTEM images of HT1 coating showing (a) Y-junction formation of CNT in the matrix, (b) 1.71 nm thick interlayer, (c) SAED pattern and FFT in the inset shown for the corresponding interfacial layer and (d) CNT arrested in a HT1 matrix including one showing a dent. SAED pattern of the amorphous region has been shown in inset.

investigated the possibility of formation of a compound during the carbothermal reaction between TiO2 and carbon. It was observed that an intermediate compound TiC_xO_y forms first, followed by a stable TiC phase. Fig. 6 (d) also shows the presence of an amorphous zone adjacent to the CNT marked in a circle. Such a phase is expected to evolve at a higher cooling rate of the order lying between 10^8 and 10^{10} K/s [39]. However, in the present investigation, no distinct reaction layer is detected in the interface of matrix and CNT in either HA1 or HT1. Thus, the CNT stay protected from harsh plasma environment. Furthermore, a dent created on CNT surface at the time of functionalisation process was filled by ceramic that further strengthens the bond with CNT. Such features were endorsed by Yamamoto et al. [40] for CNT (0.9 vol %) reinforced alumina composites consolidated by spark plasma sintering. The acid treated surface of CNT being rough surface tends to latch the CNT with ceramic interface more strongly. As a result, the composites exhibited remarkable improvement in their fracture (25%) and bending strength (27%) as compared to pure alumina [40]. It can also be observed that the interface layer thickness has been quite low. The reason for such a low thickness could be attributed to lower viscosity of titania melt as discussed and as a result, this melt, being less viscous, might have percolated through the wall of CNT by capillary action to a nearby region in the coating.

3.7. Scratch testing of coatings

During scratch test, the scratch was made on the sample and in the meantime, a plot of normal and lateral loads against scratch distance or stroke was prepared. Now, let us turn our attention to backscattered electron (BSE) image of the scratch track and X-ray dot maps of the scratched area (Fig. 7). Location of the failure was noted from the BSE image and the corresponding normal load was read from the plot. This load is known as critical load (Lc).

Bull et al. [41] have demonstrated an expression to calculate critical load and is given as:

$$L_C = \frac{A_1}{\eta \mu_C}\left[\frac{2EW}{t}\right]^{\frac{1}{2}} \quad (3)$$

where, A_1- Projected area across the indenter, η -poisson's ratio, μ_c-friction coefficient, E-elastic modulus, W-work of adhesion, and t-coating thickness. Table 4 summarises the pertinent data required to calculate work of adhesion of the coatings. The table lists location of failure of top coats and corresponding critical loads. The primary coatings properties like elastic moduli and poisson's ratio of coatings are also listed in the same table. With this information, work of adhesion for each of the coatings was calculated using equation (3).

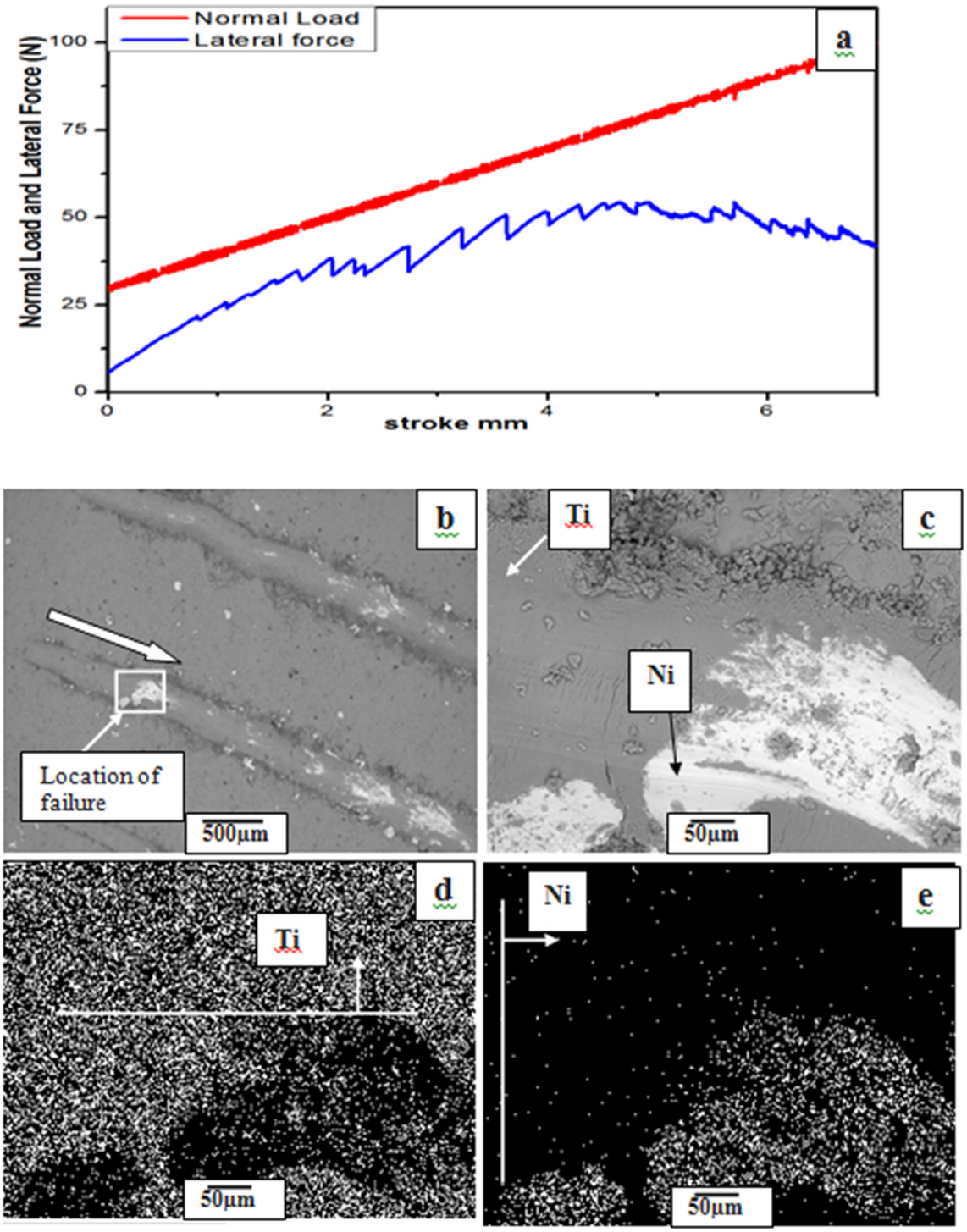

Fig. 7. Scratch test result for topcoat Crushed titania (Metco102) (a) Forces generated during scratch test. (b) BSE image at the location of failure(c) BSE image showing tensile cracks. (d) X ray dot map of titanium at the location of failure. (e) X ray dot map of nickel at the location of failure.

Fig. 7(a) shows a plot of normal load, lateral loads against stroke for HT0 coating. This plot was serrated and discontinuous, which is attributed to the presence of pores and other inhomogeneities in such thermally coatings. When an indenter passes through pore, it collapses the pore and in the process the coating is consolidated. This aspect has been reported by Ghabchi et al. [42]. Fig. 7(b) shows BSE image of the coating showing location of failure. The failed location of the coating is shown at higher magnification in Fig. 7(c). Fig. 7(d) and (e) corresponds X-ray dot map of titanium and nickel elements of the coating, respectively. Since the substrate was bond coated with Ni-5Al alloy, after perforation, Ni is exposed. Hence the dot map shows more dots of Ni than Ti. This indicates that the coating has undergone large area of spallation. The load corresponding to the failure, in turn, was used to compute work of adhesion.

Tan et al. [43] and Li and Beres [44] have demonstrated

Table 4
Scratch test results.

Top coat	Location of coating failure[a] (mm)	Elastic modulus (GPa) measured using Depth-sensing indentation	Elastic modulus (GPa) from Halpin-Tsai model	Poisson's ratio from Halpin-Tsai model	Critical load (N)	Work of adhesion (J)	% increase in Work of adhesion by measured E values
HT0	1.240 ± 0.138	122 ± 16	221.3	0.2405	43 ± 2.5	181	–
HT1	2.73 ± 0.056	143 ± 19	231.9	0.2456	57 ± 1.6	500	176
HA0	2.0 ± 0.10	110 ± 22	272.7	0.1999	50 ± 0.5	814	–
HA1	6.3 ± 0.345	135 ± 16	285.8	0.2073	93.1 ± 6.0	1104	36

[a] Measured from the scratch starting point and failure is ascertained from the x-ray dot maps.

approximately triangular profile for a Rockwell C indenter (120° angle and 200 μm radius). Hence, indenter tip radius was neglected. With the Knowledge of indenter geometry, scratch width at the point of failure was calculated as 173.2 μm, which leads to 4.33×10^{-9} m^2 cross sectional area at the point of failure. The coefficient of friction is obtained from the ratio of lateral load to normal load (Fig. 7(a)). During scratching, compressive stresses are induced in the coating ahead of moving stylus, while tensile stresses are induced at the trailing edge of stylus. This pull causes local tensile cracks to appear on the scratch track. Many researchers [16,42] demonstrated existence of such cracks. The cracks are clearly visible in Fig. 7(b) and observed on both coating as well as on bond coat. At higher normal load, these cracks tend to propagate through the splat interface and eventually dislodge the splat from the rest of the coating. Thus, the coatings fail primarily due to tensile cracks, which lead to a large area spallation as depicted in Fig. 7(c). The scratched HT1 coating figures (not shown) resemble to those of HT0 coating (Fig. 7), however it failed at a distance of 2.73 mm from the start of scratch (Table 4). These coatings have shown ~176% higher work of adhesion than HT0 coating. This is attributed to the following reasons. (1) CNT bridging arresting the crack propagation. 2) The Coatings rich in stable phase possess good mechanical properties. 3) Strong CNT/ceramic interface dictates the coating properties. 4) Such coatings exhibited ~24% improvement in their fracture toughness, which demonstrates the role of CNT in deflecting and arresting the cracks as demonstrated by Jambagi et al. [13]. 5) The load acting on the coating is transfer to stiff CNT elements rather than the coating itself. Therefore, elastic modulus (Table 4) for such coatings was improved by ~17% for titania coatings. 6) CNT bridging has been a predominant toughening mechanism for CNT reinforced thermally sprayed coatings. Fig. 8(a) shows the tensile cracks on the scratched surface. Fig. 8(b) shows a CNT bridging along with some CNT pullouts across the tensile cracks. Table 4 also shows considerable variation between theoretical and experimental elastic moduli of the coatings. The plausible explaination for such a variation is that the theoretical model fails to consider the actual heterogeneities present in the plasma sprayed coatings and thereby the model displayed overestimated results.

Laha et al. [45] reported a 78% increase in the elastic modulus in the case of plasma sprayed Al-Si alloy reinforced with 10 wt% CNT. A stiffer coating is less vulnerably susceptible to buckling, and that way it can resist large area spallation owing to compression at the leading edge of the indenter. Thus, the improvement in the critical load, and the work of adhesion of CNT reinforced coating is attributed to improvement in its cohesion and the elastic modulus. Similar observations were reported by Ghabchi et al. [42] for HVOF sprayed WC-Co coatings.

Table 4 shows a higher work of adhesion for HT1 coating than HA1 coating. The latter powder is an agglomerated one, and it is difficult to melt such powder owing to their poor heat transfer characteristics. On the other hand, titania, having the lowest melting point in this group is easier to melt. As stated earlier, the lower viscosity of HT1 coating possibly enabled a sizably voluminous number of well-engulfed CNT in it. Hence, for this reason, the coating has shown a higher stiffness and work of adhesion during the scratch test.

4. Conclusions

The plasma sprayed coatings were deposited using the CNT-doped powders. These powders were prepared by three different

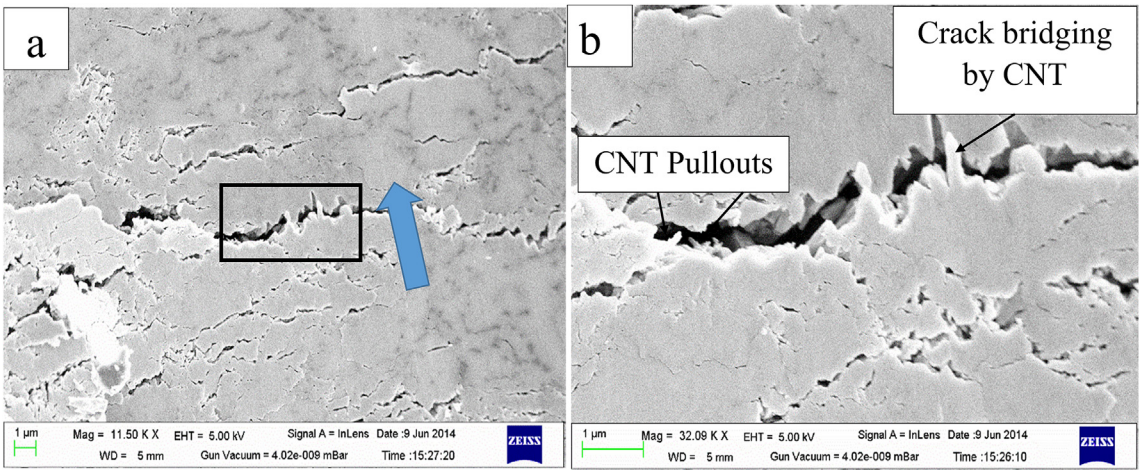

Fig. 8. Secondary electron image of the HT1 coating after the scratch test showing (a) tensile cracks. Scratch direction is shown using an arrow (b) crack bridging by CNT. Fig. (b) is a magnified view of the area enclosed by the rectangle in (a).

routes: ball milling the powders either with (wet mixing) or without alcohol (dry mixing) and heterocoagulation, a colloidal processing technique. The coatings produced from various routes have shown good microstructural integrity. The heterocoagulated coatings displayed homogenous dispersion of CNT as compared to the coatings deposited using the other two types of powders, viz., dry mixing and wet mixing. The effect of CNT dispersion on phase transformation has been examined. Owing to a homogeneous dispersion of CNT, the heterocoagulated coatings had a higher fraction of stable phase, which is known for its good mechanical properties. These coatings were further analysed for the possible interfacial reaction with the CNT. A stable phase layer was found tightly engulfing the entire CNT surface, protecting it from thermal degradation against plasma plume. Since the coatings have retained stable phase, in addition to CNT reinforcement, the effect of phase transformation on the scratch adhesion strength of the coatings was investigated. The scratch adhesion strength of heterocoagulated coatings has increased by ~36–176% as compared to that of unreinforced coatings. This has been attributed to the following three factors: First, the homogeneous dispersion of CNT in the coatings, retaining higher amount of stable phase in the coatings. Second, the strong wettability between CNT and ceramic interface and the toughening mechanism like CNT bridging mechanism. Third, the elastic modulus of the titania coatings has improved by ~17% and thus improves the stiffness of the coating.

Acknowledgement

I would like to express my sincere gratitude to the Mechanical Engineering department, IIT Kharagpur, West Bengal, India. I thank professor P.P.Bandyopadhyay, my Ph.D. superviser, for his constant encouragement to write this report. This research did not receive any specific grant from funding agencies in the public, commercial, or not-for-profit sectors.

References

[1] G. Bolelli, K. Sabiruddin, L. Lusvarghi, E. Gualtieri, S. Valeri, P. Bandyopadhyay, FIB assisted study of plasma sprayed splat–substrate interfaces: NiAl–stainless steel and alumina–NiAl combinations, Surf. Coat. Technol. 205 (2010) 363–371, http://dx.doi.org/10.1016/j.surfcoat.2010.06.057.
[2] S. Hazra, K. Sabiruddin, P. Bandyopadhyay, Plasma and HVOF sprayed WC–Co coatings as hard chrome replacement solution, Surf. Eng. 28 (2012) 37–43, http://dx.doi.org/10.1179/1743294410y.0000000009.
[3] V. Bolleddu, V. Racherla, P. Bandyopadhyay, Microstructural and tribological characterization of air plasma sprayed nanostructured alumina–titania coatings deposited with nitrogen and argon as primary plasma gases, Mater. Des. 59 (2014) 252–263, http://dx.doi.org/10.1016/j.matdes.2014.02.040.
[4] R.S. Lima, B.R. Marple, From APS to HVOF spraying of conventional and nanostructured titania feedstock powders: a study on the enhancement of the mechanical properties, Surf. Coat. Technol. 200 (2006) 3428–3437, http://dx.doi.org/10.1016/j.surfcoat.2004.10.137.
[5] K. Sabiruddin, J. Joardar, P. Bandyopadhyay, Analysis of phase transformation in plasma sprayed alumina coatings using Rietveld refinement, Surf. Coat. Technol. 204 (2010) 3248–3253, http://dx.doi.org/10.1016/j.surfcoat.2010.03.026.
[6] C.C. Stahr, S. Saaro, L.-M. Berger, J. Dubský, K. Neufuss, M. Herrmann, Dependence of the stabilization of α-alumina on the spray process, J. Therm. Spray Technol. 16 (2007) 822–830, http://dx.doi.org/10.1007/s11666-007-9107-7.
[7] J. Ilavsky, C. Berndt, H. Herman, P. Chraska, J. Dubsky, Alumina-base plasma-sprayed materials—Part II: phase transformations in aluminas, J. Therm. Spray Technol. 6 (1997) 439–444, http://dx.doi.org/10.1007/s11666-997-0028-2.
[8] M.I. Mendelson, Theoretical evaluation of wear in plasma-sprayed TiO 2 against grey cast iron, Wear 50 (1978) 71–83, http://dx.doi.org/10.1016/0043-1648(78)90246-6.
[9] P. He, G. Ma, H. Wang, Q. Yong, S. Chen, Microstructure and mechanical properties of a novel plasma-spray TiO2 coating reinforced by CNTs, Ceram. Int. 42 (2016) 13319–13325, http://dx.doi.org/10.1016/j.ceramint.2016.05.073.
[10] K. Balani, S.R. Bakshi, Y. Chen, T. Laha, A. Agarwal, Role of powder treatment and carbon nanotube dispersion in the fracture toughening of plasma-sprayed aluminum oxide—carbon nanotube nanocomposite, J. Nanosci. Nanotechnol. 7 (2007) 3553–3562, http://dx.doi.org/10.1166/jnn.2007.851.
[11] K. Balani, A. Agarwal, Process map for plasma sprayed aluminum oxide–carbon nanotube nanocomposite coatings, Surf. Coat. Technol. 202 (2008) 4270–4277, http://dx.doi.org/10.1016/s0026-0576(08)80204-8.
[12] S.C. Jambagi, N. Sarkar, P. Bandyopadhyay, Preparation of carbon nanotube doped ceramic powders for plasma spraying using heterocoagulation method, J. Eur. Ceram. Soc. 35 (2015) 989–1000, http://dx.doi.org/10.1016/j.jeurceramsoc.2014.10.017.
[13] S.C. Jambagi, S. Kar, P. Brodard, P. Bandyopadhyay, Characteristics of plasma sprayed coatings produced from carbon nanotube doped ceramic powder feedstock, Mater. Des. 112 (2016) 392–401, http://dx.doi.org/10.1016/j.matdes.2016.09.095.
[14] M.L. Gualtieri, M. Prudenziati, A.F. Gualtieri, Quantitative determination of the amorphous phase in plasma sprayed alumina coatings using the Rietveld method, Surf. Coat. Technol. 201 (2006) 2984–2989, http://dx.doi.org/10.1016/j.surfcoat.2006.06.009.
[15] X. Wang, Z. Liu, H. Liao, D. Klein, C. Coddet, Deoxidisation and phase analysis of plasma sprayed TiO 2 by X-ray Rietveld method, Thin Solid Films 473 (2005) 177–184, http://dx.doi.org/10.1016/j.tsf.2004.02.092.
[16] S. Hazra, P. Bandyopadhyay, Scratch induced failure of plasma sprayed alumina based coatings, Mater. Des. 35 (2012) 243–250, http://dx.doi.org/10.1016/j.matdes.2011.09.014.
[17] R. Rao, R. Podila, R. Tsuchikawa, J. Katoch, D. Tishler, A.M. Rao, M. Ishigami, Effects of layer stacking on the combination Raman modes in graphene, ACS Nano 5 (2011) 1594–1599, http://dx.doi.org/10.1021/nn1031017.
[18] W.C. Oliver, G.M. Pharr, Measurement of hardness and elastic modulus by instrumented indentation: advances in understanding and refinements to methodology, J. Mater. Res. 19 (2004) 3–20, http://dx.doi.org/10.1557/jmr.2004.0002.
[19] S. Brossard, P. Munroe, M. Hyland, Microstructural study of splat formation for HVOF sprayed NiCr on pre-treated aluminum substrates, J. Therm. Spray Technol. 19 (2010) 1001–1012, http://dx.doi.org/10.1007/s11666-010-9482-3.
[20] K. Ramachandran, V. Selvarajan, P. Ananthapadmanabhan, K. Sreekumar, Microstructure, adhesion, microhardness, abrasive wear resistance and electrical resistivity of the plasma sprayed alumina and alumina–titania coatings, Thin Solid Films 315 (1998) 144–152, http://dx.doi.org/10.1016/s0040-6090(97)00738-4.
[21] O. Sarikaya, Effect of some parameters on microstructure and hardness of alumina coatings prepared by the air plasma spraying process, Surf. Coat. Technol. 190 (2005) 388–393, http://dx.doi.org/10.1016/j.surfcoat.2004.02.007.
[22] K. Sabiruddin, P. Bandyopadhyay, G. Bolelli, L. Lusvarghi, Variation of splat shape with processing conditions in plasma sprayed alumina coatings, J. Mater. Process. Technol. 211 (2011) 450–462, http://dx.doi.org/10.1016/j.jmatprotec.2010.10.020.
[23] D. Bessinger, in: Cooling Characteristics of High Titania Slags, University of Pretoria, South Africa, 2000. Ph.D. Thesis.
[24] M. Wang, D. Chen, Z. Chen, Y. Wu, F. Wang, N. Ma, H. Wang, Mechanical properties of in-situ TiB 2/A356 composites, Mater. Sci. Eng. A 590 (2014) 246–254, http://dx.doi.org/10.1016/j.msea.2013.10.021.
[25] T. Tayeh, J. Douin, S. Jouannigot, M. Zakhour, M. Nakhl, J.-F. Silvain, J.-L. Bobet, Hardness and Young's modulus behavior of Al composites reinforced by nanometric TiB 2 elaborated by mechanosynthesis, Mater. Sci. Eng. A 591 (2014) 1–8, http://dx.doi.org/10.1016/j.msea.2013.10.065.
[26] O. Kovářík, J. Siegl, J. Nohava, P. Chraska, Young's modulus and fatigue behavior of plasma-sprayed alumina coatings, J. Therm. Spray Technol. 14 (2005) 231–238, http://dx.doi.org/10.1361/105996304523809.
[27] A.M. Díez-Pascual, A.L. Díez-Vicente, Effect of TiO 2 nanoparticles on the performance of polyphenylsulfone biomaterial for orthopaedic implants, J. Phys. Chem. B 2 (2014) 7502–7514, http://dx.doi.org/10.1039/c4tb01101e.
[28] S.R. Bakshi, V. Singh, K. Balani, D.G. McCartney, S. Seal, A. Agarwal, Carbon nanotube reinforced aluminum composite coating via cold spraying, Surf. Coat. Technol. 202 (2008) 5162–5169, http://dx.doi.org/10.1016/j.surfcoat.2008.05.042.
[29] Y. Xie, H. Hawthorne, Wear mechanism of plasma-sprayed alumina coating in sliding contacts with harder asperities, Wear 225 (1999) 90–103, http://dx.doi.org/10.1016/s0043-1648(98)00351-2.
[30] P. Ctibor, K. Neufuss, P. Chraska, Microstructure and abrasion resistance of plasma sprayed titania coatings, J. Therm. Spray Technol. 15 (2006) 689–694, http://dx.doi.org/10.1361/105996306x146749.
[31] P. Zhao, G. Shi, Study of Poisson's ratios of graphene and single-walled carbon nanotubes based on an improved molecular structural mechanics model, Struct. Longev. 5 (2011) 49–58.
[32] D.A. Hanaor, C.C. Sorrell, Review of the anatase to rutile phase transformation, J. Mater. Sci. 46 (2011) 855–874, http://dx.doi.org/10.1007/s10853-010-5113-0.
[33] R.D. Shannon, J.A. Pask, Kinetics of the anatase-rutile transformation, J. Am. Ceram. Soc. 48 (1965) 391–398, http://dx.doi.org/10.1111/j.1151-2916.1965.tb14774.x.
[34] C. Lee, H. Choi, C. Lee, H. Kim, Photocatalytic properties of nano-structured TiO 2 plasma sprayed coating, Surf. Coat. Technol. 173 (2003) 192–200, http://dx.doi.org/10.1016/s0257-8972(03)00509-7.
[35] S. Aruna, N. Balaji, J. Shedthi, V.W. Grips, Effect of critical plasma spray parameters on the microstructure, microhardness and wear and corrosion resistance of plasma sprayed alumina coatings, Surf. Coat. Technol. 208 (2012) 92–100, http://dx.doi.org/10.1016/j.surfcoat.2012.08.016.
[36] A.K. Keshri, K. Balani, S.R. Bakshi, V. Singh, T. Laha, S. Seal, A. Agarwal,

Structural transformations in carbon nanotubes during thermal spray processing, Surf. Coat. Technol. 203 (2009) 2193–2201, http://dx.doi.org/10.1016/j.surfcoat.2009.02.013.
[37] A.K. Keshri, J. Huang, V. Singh, W. Choi, S. Seal, A. Agarwal, Synthesis of aluminum oxide coating with carbon nanotube reinforcement produced by chemical vapor deposition for improved fracture and wear resistance, Carbon 48 (2010) 431–442, http://dx.doi.org/10.1016/j.carbon.2009.08.046.
[38] J. Kim, S. Kang, Stable phase domains of the TiO 2–Ti 3 O 5–Ti 2 O 3–TiO–Ti (C x O y)–TiC system examined experimentally and via first principles calculations, J. Mater. Chem. A 2 (2014) 2641–2647, http://dx.doi.org/10.1039/c3ta14633b.
[39] L. Li, B. Kharas, H. Zhang, S. Sampath, Suppression of crystallization during high velocity impact quenching of alumina droplets: observations and characterization, Mater. Sci. Eng. A 456 (2007) 35–42, http://dx.doi.org/10.1016/j.msea.2006.11.132.
[40] G. Yamamoto, M. Omori, T. Hashida, H. Kimura, A novel structure for carbon nanotube reinforced alumina composites with improved mechanical properties, Nanotechnology 19 (2008) 315708, http://dx.doi.org/10.1088/0957-4484/19/31/315708.
[41] S. Bull, D. Rickerby, A. Matthews, A. Leyland, A. Pace, J. Valli, The use of scratch adhesion testing for the determination of interfacial adhesion: the importance of frictional drag, Surf. Coat. Technol. 36 (1988) 503–517, http://dx.doi.org/10.1016/0257-8972(88)90178-8.
[42] A. Ghabchi, S. Sampath, K. Holmberg, T. Varis, Damage mechanisms and cracking behavior of thermal sprayed WC–CoCr coating under scratch testing, Wear 313 (2014) 97–105, http://dx.doi.org/10.1016/j.wear.2014.02.017.
[43] Y. Tan, S. Jiang, D. Yang, Y. Sheng, Scratching of Al 2 O 3 under pre-stressing, J. Mater. Process. Technol. 211 (2011) 1217–1223, http://dx.doi.org/10.1016/j.jmatprotec.2011.02.005.
[44] J. Li, W. Beres, Three-dimensional finite element modelling of the scratch test for a TiN coated titanium alloy substrate, Wear 260 (2006) 1232–1242, http://dx.doi.org/10.1016/j.wear.2005.08.008.
[45] T. Laha, Y. Chen, D. Lahiri, A. Agarwal, Tensile properties of carbon nanotube reinforced aluminum nanocomposite fabricated by plasma spray forming, Compos. Part A 40 (2009) 589–594, http://dx.doi.org/10.1016/j.compositesa.2009.02.007.